miRNA-30 Family Members Inhibit Breast Cancer Invasion, Osteomimicry, and Bone Destruction by Directly Targeting Multiple Bone Metastasis–Associated Genes

Martine Croset[1], Francesco Pantano[1,2], Casina W.S. Kan[1], Edith Bonnelye[1], Françoise Descotes[3], Catherine Alix-Panabières[4], Charles-Henri Lecellier[5], Richard Bachelier[1], Nathalie Allioli[6], Saw-See Hong[7], Kai Bartkowiak[8], Klaus Pantel[8], and Philippe Clézardin[1]

Abstract

miRNAs are master regulators of gene expression that play key roles in cancer metastasis. During bone metastasis, metastatic tumor cells must rewire their biology and express genes that are normally expressed by bone cells (a process called osteomimicry), which endow tumor cells with full competence for outgrowth in the bone marrow. Here, we establish miR-30 family members miR-30a, miR-30b, miR-30c, miR-30d, and miR-30e as suppressors of breast cancer bone metastasis that regulate multiple pathways, including osteomimicry. Low expression of miR-30 in primary tumors from patients with breast cancer were associated with poor relapse-free survival. In addition, estrogen receptor (ER)-negative/progesterone receptor (PR)-negative breast cancer cells expressed lower miR-30 levels than their ER/PR-positive counterparts. Overexpression of miR-30 in ER/PR-negative breast cancer cells resulted in the reduction of bone metastasis burden *in vivo*. *In vitro*, miR-30 did not affect tumor cell proliferation, but did inhibit tumor cell invasion. Further-

more, overexpression of miR-30 restored bone homeostasis by reversing the effects of tumor cell–conditioned medium on osteoclastogenesis and osteoblastogenesis. A number of genes associated with osteoclastogenesis stimulation (*IL8*, *IL11*), osteoblastogenesis inhibition (*DKK-1*), tumor cell osteomimicry (*RUNX2*, *CDH11*), and invasiveness (*CTGF*, *ITGA5*, *ITGB3*) were identified as targets for repression by miR-30. Among these genes, silencing *CDH11* or *ITGA5* in ER-/PR-negative breast cancer cells recapitulated inhibitory effects of miR-30 on skeletal tumor burden *in vivo*. Overall, our findings provide evidence that miR-30 family members employ multiple mechanisms to impede breast cancer bone metastasis and may represent attractive targets for therapeutic intervention.

Significance: These findings suggest miR-30 family members may serve as an effective means to therapeutically attenuate metastasis in triple-negative breast cancer. *Cancer Res; 78(18); 5259–73. ©2018 AACR.*

Introduction

Breast cancer has a particular propensity to spread to the skeleton and around 70%–80% of patients with advanced disease

develop bone metastases. Once metastatic cells reach the bone marrow, they alter the functions of bone-resorbing (osteoclasts) and bone-forming (osteoblasts) cells, promoting skeletal destruction (1). Antiresorptive therapies (bisphosphonates, denosumab) are drugs that inhibit bone destruction (2). However, despite these treatments, a significant proportion of patients still experience progression of the metastatic bone disease (2). To develop more effective bone-targeted therapies, a number of genes and signaling pathways specifically associated with breast cancer bone metastasis came under intense scrutiny during the past two decades (3–5). In a similar vein, miRNAs, which are master regulators of gene expression, have emerged as key players in cancer progression and a whole new field of possible therapeutic interventions, including for bone metastasis, is coming out (6, 7).

Small noncoding miRNAs bind to target mRNAs, resulting in translational repression or mRNA degradation (6). miRNAs that are frequently downregulated in cancer and metastasis have been reported to act as metastasis suppressors (6). For example, the miR-200 family members directly target *ZEB1* mRNA, a transcriptional repressor of the cytoskeletal rearrangement protein E-cadherin (6). As a consequence of miR-200 downregulation, *ZEB1* upregulation promotes epithelial-to-mesenchymal transition (EMT) in cancer metastasis (6). Conversely, some miRNAs are

[1]INSERM, UMR_S1033, University Lyon 1, Lyon, France. [2]Medical Oncology Department, Campus Bio-Medico University of Rome, Rome, Italy. [3]Service de Biochimie Biologie Moléculaire, Hospices Civils de Lyon, Lyon, France. [4]Laboratory of Rare Human Circulating Cells (LCCRH), University Medical Centre, Montpellier, France. [5]Université Montpellier 1, Montpellier, France. [6]Institut des Sciences Pharmaceutiques et Biologiques (ISPB)-Faculté de Pharmacie de Lyon, University Claude Bernard Lyon 1. Centre de Recherche en Cancérologie de Lyon, Inserm U1052, CNRS UMR5286, Lyon, France. [7]University Lyon 1, UMR 754-INRA-EPHE, Lyon, France. [8]Department of Tumor Biology, University Medical Centre Hamburg-Eppendorf, Hamburg, Germany.

upregulated in tumors, and they act as promoters of metastatic progression. For instance, miR-10b and miR-21 are overexpressed in cancer (6) and we have shown that their increased expression in breast cancer promotes tumor cell invasion and survival in the bone marrow, thereby facilitating bone metastasis formation (8, 9). Other miRNAs are emerging as important mediators of multiple mechanisms of bone metastasis, including cancer cell invasion (miR-31, miR-373), tumor–bone cell interactions (miR-34a, miR-141, miR-219) and overt skeletal outgrowth (miR-16, miR-204, miR-211, miR-218, miR-378, miR-379; refs. 10, 11). Conditioned media derived from breast and bladder carcinomas activate a miRNA response signature in osteoclasts that correlate with bone metastasis burden (12). However, the importance of miRNAs in regulating bone metastasis formation is only beginning to be uncovered.

Metastatic tumor cells growing in distant organs must rewire their biology to meet the demands of the organ colonized, thus modifying their primary properties (13). To adapt to the bone microenvironment, we have shown that breast cancer cells express bone-associated genes (CTSK, SPARC, CDH11, CX43, DKK1, RUNX2) that are normally expressed by osteoblasts or osteoclasts. This process is called osteomimicry (14, 15). Previous studies in bone physiology have shown that miR-30 family members regulate osteoblast differentiation by targeting transcription factor RUNX2 (16, 17). Here, we hypothesized that miR-30 family members regulate tumor cell osteomimicry.

The contribution of miR-30 family members in the multiple steps of bone metastasis formation is currently unknown. The miR-30 family consists of 5 members: miR-30a through miR-30e. They are located at three different chromosomal regions: 1p34.2 (miR-30c and miR-30e), 6q13 (miR-30a), and 8q24.22 (miR-30b and miR-30d; ref. 18). In cancer and metastasis, miR-30 family members have been generally ascribed a tumor suppressor role, while in some circumstances they may act as oncogenes (19–31). More specifically, miR-30a inhibits primary tumor growth and/or lung metastasis formation in several cancer types (breast, prostate, thyroid and colon carcinomas, osteosarcoma; refs. 19–23). miR-30b and miR-30c suppress in vivo lung metastasis of liver and colon cancer, respectively (24, 25). miR-30c also inhibits breast tumor chemotherapy resistance and multiple myeloma growth and is a predictor for clinical benefit to endocrine therapy in advanced breast cancer (26–28). Conversely, miR-30c was reported to promote breast cancer cell invasion in vitro (29). A similar oncogenic role has been reported for miR-30b/d in melanoma, by promoting tumor cell invasion and metastatic dissemination in vivo (30). miR-30e suppresses proliferation of hepatocarcinoma cells in vitro (31).

In this study, we provide evidence that miR-30 family members (miR-30a, miR-30b, miR-30c, miR-30d and miR-30e) act as tumor suppressor genes in breast cancer bone metastasis. We show that miR-30 overexpression in human breast cancer cells reduces tumor cell invasion, osteomimicry, and bone destruction in vivo by directly targeting multiple genes.

Materials and Methods

Cell lines and cell culture

The human breast cancer lines were obtained from the ATCC [MDA-MB-231 (year 2014), T47-D (year 2012), MCF-7 (year 2012), BT-474 (year 2010), ZR-751 (year 2010) SK-BR3 (year 2008)] and Hs-578T (year 2010). The human MDA-B02 cell line (MDA-B02) is a subpopulation of the MDA-MB-231 breast cancer cell line that was selected for the high efficiency with which it metastasizes to bone in animals (32). All of these cell lines were tested for authentication by DNA fingerprinting using short tandem repeat (STR) method in 2014. BC-M1 is a disseminated tumor cell line obtained from a bone marrow aspirate of a patient with breast cancer with no clinical signs of distant metastasis at the time of primary tumor resection (33, 34). Cell culture conditions for growing each of these human breast cancer cell lines are described in the Supplementary Methods section. Cell cultures were routinely tested for Mycoplasma by measuring the luminescence intensity from cell culture supernatants, using the MycoAlert PLUS Mycoplasma Detection Kit (Lonza).

Cohort of patients with breast cancer

Patients ($n = 109$) who were included in the study were free of treatment at the time of surgery and primary breast tumors had no inflammatory features (35). Studies involving human primary breast tumors were carried out according to the Declaration of Helsinki. Patient studies were performed after approval by an institutional review board at Centre Hospitalier Lyon-Sud (CHLS, Lyon, France). The investigators obtained informed written consent from the subjects. Clinicopathologic characteristics of the cohort are shown in Supplementary Table S1 and methods for the processing of patient-derived tumor tissue are described in the Supplementary Methods section.

Plasmid constructs

The retroviral vectors containing genomic sequences of miR-30b, miR-30d, miR-30b-d, miR-30b-c, or miR-30a-b-c-d-e were constructed by inserting the PCR-amplified miR-30 genomic DNA into the HindIII/EcoRI multiple cloning site of pmiRVec. Genomic DNA was extracted from MDA-MB-231 with Nucleo-Spin Tissue kit (Macherey-Nagel) and used as PCR template in presence of appropriate primers to generate PCR products (see Supplementary Methods section). The luciferase reporter plasmids were constructed by insertion of DNA fragments derived from the 3′UTR of CTGF, ITGA5 and of the 364-base pairs of CDH11 ORF into the psicheck-2 dual luciferase reporter vector (Promega). The inserted DNA fragments were PCR-amplified from genomic MDA-MB-231, using appropriate primers (see Supplementary Methods section). For the construction of deletion mutants we used a QuikChange Lightning Site-Directed Mutagenesis Kit (Stratagene) with the generated psiCHECK-2 vectors, as the template, and the appropriated primers (see Supplementary Methods).

Cell transduction and transfection

MDA-B02 cells were transduced using the pantropic retroviral expression packaging system (Clontech Laboratories, Takara Bio Company). Briefly, the GP2-293 cell line, which has the viral gag and pol genes incorporated in its genome, was transfected with the pantropic VSV-G envelope vector and the human miR-30 genomic DNA inserted in the retroviral pmiRVec vector (kindly provided by Dr. R. Agami, The Netherlands Cancer Institute, Amsterdam, the Netherlands). Virus particles were collected 72 hours after transfection, filtered, and used to transduce recipient cells in presence of 8 μg/mL polybrene. Transduced cells were selected with 5 μg/mL blasticidin.

Transient overexpression or downregulation of miR-30s in MDA-B02 and MDA-MB-231 cells was achieved by transfecting

cells with chemically modified double-stranded RNAs that mimic endogenous miRs (miRNA-mimics, Applied Biosystems) or single-stranded RNA molecules designed to specifically inhibit endogenous miRNAs (miRNA-inhibitors, Applied Biosystems). Both cell lines were transfected with 10 nmol/L of each miR-30s mimics or antagonist sequences or with 50 nmol/L of negative scramble controls (Applied Biosystems). These oligonucleotides were incubated with 10^6 cells in appropriated medium, in the presence of HiPerFect transfection reagent (Qiagen) for 30 minutes at 37°C in a 5% CO_2 incubator prior to cell plating in 6-well plates. Transfected cells were then grown in culture for 72 hours before cell assays. The efficiency of oligonucleotide delivery into these tumor cells was assessed using cell transfection with Alexa-Fluor488–conjugated oligonucleotides followed by flow cytometry analysis of fluorescently-labeled transfected cells. HEK-293T cells were transfected with the appropriate reporter plasmids (see Supplementary Methods section) using X-tremeGene reagent (Promega).

MC3T3-E1 osteoblastic cells were also transiently transfected by equimolar concentrations of each miR-30 mimic (10 nmol/L each) or corresponding control (50 nmol/L; Applied BioSystems) by incubating cells in suspension with oligonucleotides in the presence of HiPerfect (Qiagen) for 30 minutes at 37°C prior to cell plating.

Hs-578T, MDA-MB-231, and MDA-B02 cells expressing luciferase2 (Hs-578T-luc2, MDA-MB-231-luc2, and MDA-B02-luc2) were obtained by retroviral transduction of tumor cells with pmiRVec containing the luciferase2 ORF, followed by blasticidin selection. Stable silencing of *ITGA5* in Hs-578T-luc2 cells and of *CDH11* in MDA-B02-luc2, MDA-MB-231-luc2 and Hs-578T-luc2 cells was achieved by transducing these cells with lentiviral plasmids containing hairpin shRNAs targeting *ITGA5 or CDH11*. A universal nontargeting shRNA was used as a negative control (pZIP-hCMV-shRNA-miR lentiviral vector, Transomic Technologies). shRNA designs (see Supplementary Methods) were predicted using the proprietary shERWOOD algorithm (Dr. Gregory Hannon's laboratory at Cold Spring Harbor Laboratory) and cloned into the UltramiR scaffolds for optimal shRNA processing according to the constructor. Lentiviral particles were obtained by transfecting the Lenti-X 293T Cell Line with the Lenti-X HTX Packaging System and the pZIP-hCMV-shRNA plasmid in presence of Xfect Transfection Reagent, according to the constructor guidelines (Takara, Clontech Laboratories). Lentiviral particles were incubated with tumor cells seeded on the RetroNectin Reagent in complete medium containing tetracycline-free FBS (Takara, Clontech Laboratories). Transduced tumor cells were subjected to selection with 2 μg/mL puromycin.

Real-time RT-PCR

Total RNA from human breast tumor and MC3T3-E1 cells was extracted using the Nucleospin RNA kit based on RNA adsorption on silica membranes and further treated by rDNAse (Macherey Nagel). Total RNA from murine osteoclasts was extracted with the miRNeasy Micro Kit (Qiagen; ref. 8). cDNA was produced from 1 μg of total RNA using the iScript cDNA Synthesis Kit (Bio-Rad). Real-time quantitative PCR reactions were performed using a SYBR Green qPCR kit (SYBR Green qPCR Super Mix, Life Technologies) on Mastercycler RealPlex (Eppendorf GmbH). Relative gene expression levels were normalized according to the C_t value of the gene encoding the ribosomal protein L32 and results were expressed as fold differences equal to $2^{-\Delta\Delta C_t}$.

Analysis of miRNA expression

TaqMan miRNA assays (Applied Biosystems, Life Technologies) were used to quantify miRNA and RNU48 and Snu6 levels after extraction by cell homogenization in Qiazol reagent followed by extraction on silica column (miRNeasy Micro Kit, Qiagen; ref. 8). Ten nanograms of total RNA were reverse-transcribed using the MultiScribe reverse transcriptase and 50 nmol/L stem-loop RT primers specific for miRNAs and the endogenous control RNU48. Mature miRNAs were amplified using the TaqMan 2× universal PCR Master Mix and levels were expressed as fold differences equal to $2^{-\Delta\Delta C_t}$. Analysis of miRNA expression in primary breast tumors was performed on TaqMan 96-well custom plates after multiplexed reverse transcription (RT; Supplementary Methods section). miRNA profiling of breast cancer cell lines was performed by real-time PCR on TaqMan Low Density Array Human MicroRNA Panels A and B (Applied Biosystems; See Supplementary Methods section). ΔC_t values were calculated using RNU48 and Snu6 as endogenous controls with the RQ manager (Applied Biosystems).

Dual luciferase reporter assay

HEK-293T cells were transfected by incubating the cells overnight with 10 nmol/L of each miR-30 mimics or with 50 nmol/L of negative scramble controls followed by transfection with the appropriate reporter plasmids using X-tremeGene reagent (Promega). Forty-eight hours after transfection, cells were harvested in lysis buffer and subjected to luciferase reporter assay using Dual-Glo Luciferase Reporter Assay System (Promega). *Renilla* luciferase activity was normalized to corresponding firefly luciferase activity and plotted as a ratio between the two values.

Western blotting

Total protein cell extracts were lysed in RIPA buffer (Sigma) containing a cocktail of protease inhibitor (Roche). Protein cell extracts were electrophoresed on a 4%–12% gradient SDS-polyacrylamide gel (Life technologies), then transferred onto nitrocellulose membranes (Millipore), and proteins were probed with a primary antibody against CDH11 (human cadherin-11 polyclonal antibody, 1/2,000 dilution; R&D Systems), ITGA5 (mouse anti-α5 integrin, 1/1,000 dilution; Millipore), ITGB3 (D7 × 3P rabbit anti-integrin beta-3 mAb, 1/5,000 dilution; Cell Signaling Technology), Twinfilin-1 (rabbit polyclonal antibody, 1/2,000 dilution; Cell Signaling Technology), CTGF (D8Z8U rabbit mAb, 1/2,000 dilution; Cell Signaling Technology), CX43 (CX43/GJA1 rabbit polyclonal antibody, 1/5,000 dilution; Abcam), RunX2 (mouse mAb, 1/2,000 dilution, Abcam), and β-tubulin (Cl B-512, 1/5,000 dilution; Sigma), according to manufacturer's instructions. After incubation with primary antibodies, membranes were incubated with horseradish peroxide (HRP)-conjugated donkey anti-rabbit or anti-mouse secondary antibodies (1/2,000 dilution; Amersham), and immunostaining was performed with enhanced chemiluminescence (ECL) detection system (Perkin Elmer).

ELISA

Conditioned media from MDA-B02-Ctrl and MDA-B02-miR-30s cells were collected and IL8 and IL11 levels measured by ELISA, according to the manufacturer's instructions (CliniSciences).

Cell invasion assay

Experiments were conducted in 24-well plates with 8-μm diameter pore-size inserts, previously coated with 100 μL basement membrane Matrigel (0.3 mg/mL), as described previously (8).

Tumor cell enumeration assay

Cell growth curves were obtained after seeding the cells (10^4 per well) into 12-well plates and culturing them up to 96 hours. Cells were harvested with trypsin at various time points and cell suspensions were then counted by flow cytometry using the True Volumetric Absolute Counting technique (Partec Instruments).

Osteoclastogenesis assay

Experiments were conducted as described previously (8, 36), using murine bone marrow cells cultured in the presence of M-CSF (20 ng/mL; R&D Systems) and RANK-L (30 ng/mL; Pepro-Tech), alone or in the presence of conditioned medium from transfectants (25 μg/mL). After 7 days in culture, mature osteoclasts were enumerated under a microscope on the basis of the number of nuclei ($\geq$ three nuclei) and on the tartrate-resistant acid phosphatase (TRAP) activity. Results were expressed as the number of osteoclasts per well.

Osteoblastogenesis assay

Experiments were conducted as described previously (37). Briefly, MC3T3-E1 osteoblastic cells were seeded in 12-well plates (10^5 cells/well) and cultured in αMEM medium containing 10% FBS and 50 μg/mL ascorbic acid from day 1 to day 8, at which time 10 mmol/L β-glycero-phosphate (Sigma-Aldrich) was added to the culture medium and cells were further cultured with or without conditioned medium from transfectants (25 μg/mL protein). At day 21, bone-mineralized nodules were fixed and stained with von Kossa staining. Alternatively, nodules were harvested in lysis buffer for RNA extraction.

Animals

Four-week-old female BALB/c nude mice were purchased from Janvier Laboratories. Animals were maintained in a 12-hour light–dark cycle and given free access to food and water. All procedures involving animals, including housing and care, the method by which they were sacrificed, and experimental protocols were conducted in accordance with approval of Ethical Committee (CEEA-55 *Comité d'Ethique en Expérimentation Animale*) under project licence DR2016-15, University Claude Bernard Lyon-1 (Lyon, France).

Animal studies

Tumor xenograft experiments were conducted as described previously (8, 36). Female Balb/c nude mice were inoculated subcutaneously with MDA-B02 transfectants (10^6 cells in 50 μL PBS). Tumor size was calculated by external measurement of the width (m_1) and length (m_2) of tumor xenografts using a Vernier caliper. Tumor volume (TV) was calculated using the equation $TV = (m_1{}^2 \times m_2)/2$. At the end of the protocols, mice were sacrificed and tumors collected, then prepared for IHC.

Bone metastasis experiments were conducted, as described previously (8, 32). Transfectants (5×10^5 cells in 100 μL PBS) were injected into the tail artery of anesthetized nude mice. Radiographs of anesthetized animals were taken weekly using a MX-20 cabinet X-ray system (Faxitron X-ray Corporation). Osteo-lytic lesions were identified on radiographs as radiolucent lesions in the bone. The area of osteolytic lesions was measured using a computerized image analysis system, and the extent of bone destruction per leg was expressed in square millimeters. For measurement of skeletal tumor burden, bioluminescence imaging of animals was performed weekly using the Nightowl imaging system (Berthold). On day 32 after tumor cell inoculation, anesthetized mice were sacrificed by cervical dislocation after radiography and bioluminescence imaging.

Bone histology, histomorphometry, and IHC

Bone histology and histomorphometric analysis of bone tissue sections were performed as described previously (8, 36). The bone volume (BV)/tissue volume (TV) and tumor volume (TuV)/soft tissue volume (STV) ratios represent the percentages of bone and tumor tissue, respectively. The *in situ* detection of osteoclasts was performed on TRAP-stained longitudinal paraffin-embedded medial sections of tibial metaphysis, using a commercial kit (Sigma). The resorption surface (Oc.S/BS) was calculated as the ratio of TRAP-positive trabecular bone surface (Oc.S) to the total bone surface (BS) using the image analysis system MorphoExpert (Explora-nova).

For IHC, tumor tissue sections were incubated with a mouse anti-human Ki-67 mAb (DakoCytomation) or a rabbit polyclonal anti-CD31 antibody (AnaSpec) that specifically recognize proliferative cells and blood vessels, respectively. The mitotic index and tumor microvessel density were quantified, as described previously (8).

Statistical analysis

All data were analyzed using GraphPad Prism 5 software (version5.2; GraphPad Software). Pairwise comparisons were carried out by performing nonparametric Mann–Whitney *U* test, one-way ANOVA, *post hoc* Bonferroni test and Student *t* test, as indicated in figures and tables. All tests were two-sided, and *P* values less than 0.05 were considered statistically significant.

Results

miR-30s are downregulated in human osteotropic breast cancer cell lines, and their low expression levels in primary breast tumors are associated with poor relapse-free survival in patients

We compared the miRNA expression profile of human MDA-MB-231 breast cancer cells with that of MDA-B02, a cell subpopulation that was previously selected *in vivo* on the basis of its high and selective capacity to colonize bones in mice (32), and of BC-M1, a breast cancer cell line that was established from disseminated tumor cells in the bone marrow of a patient with no sign of metastasis at the time of surgery (33). A total of 152 miRNAs were significantly up- or downregulated in these three breast cancer cell lines (Fig. 1A). For example, expression levels of miR-200 family members (miR-200a, miR-200b, miR-200c, and miR-429) and of miR-138 and miR-204, two metastasis-suppressing miRNAs, were markedly reduced in MDA-B02 and BC-M1 cells, compared with MDA-MB-231 cells (Fig. 1A). This was in agreement with the mesenchymal phenotype of these osteotropic cell lines that highly expressed CD44 and were CD24 negative (Supplementary Fig. S1). This difference was accompanied by increased expression of EMT-inducing transcription factors *ZEB1, ZEB2, SNAI1* (snail) and *SNAI2* (slug) and of mesenchymal
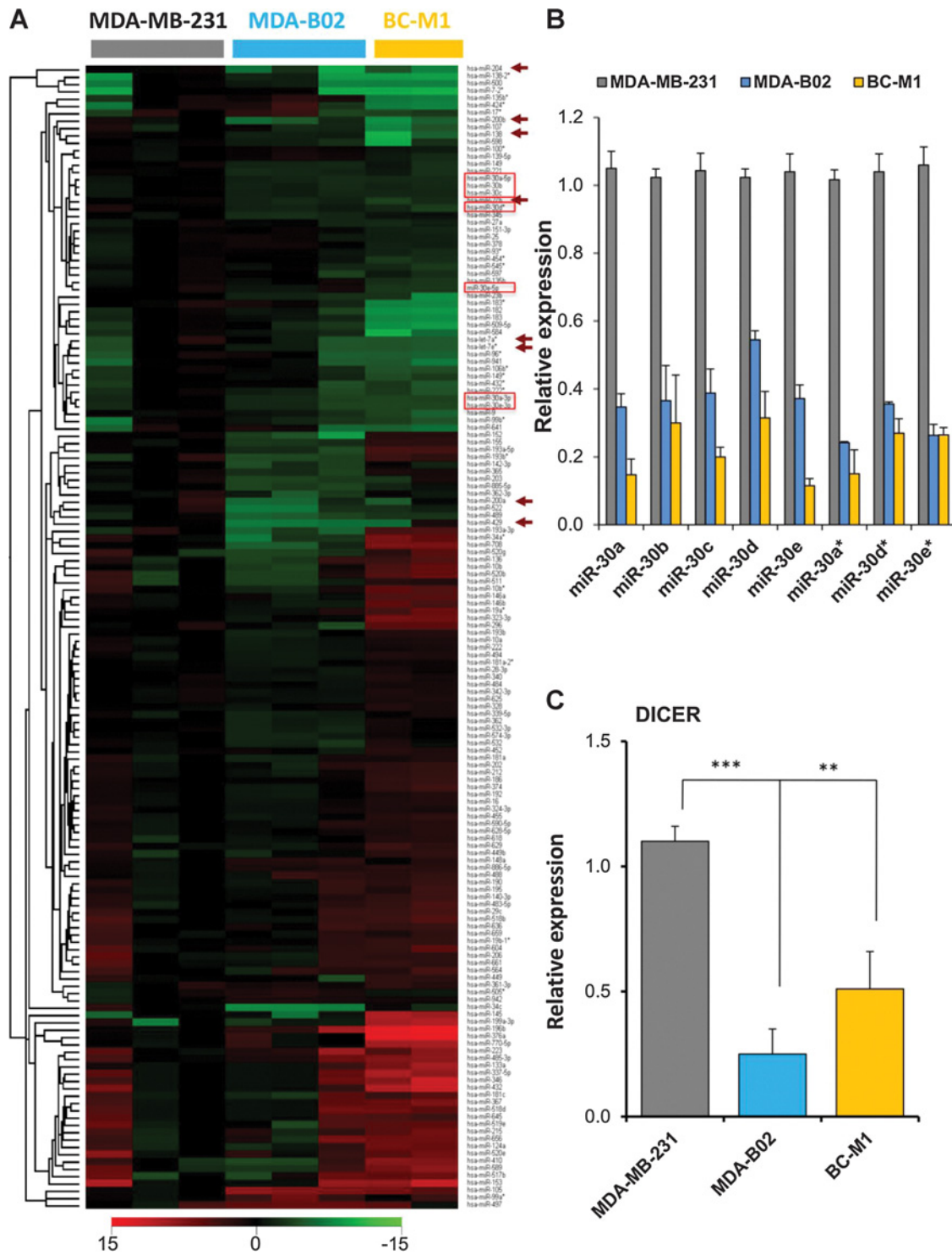
Figure 1.
miRNA profiling of human MDA-MB-231 breast cancer cells with that of osteotropic MDA-B02 and BC-M1 breast cancer cells. **A,** Heatmap diagram with two-way hierarchical clustering of miRNAs and breast cancer cell lines. Each row represents a miRNA and each column represents a breast cancer cell sample. The color scale at the bottom illustrates the relative expression level of each miRNA across all samples; red and green are expression levels above and below the mean, respectively. Black is the mean expression level. miR-30 family members are shown in red boxes. Metastasis-suppressing miRNAs, which are relevant to EMT and cancer cell stemness, are indicated by red arrows. Values are representative of the relative quantification of miRNAs measured by TaqMan Low Density Array in three separated cell cultures. ΔC_t values were calculated using RNU48 and Snu6 as endogenous controls with the RQ manager (Applied Biosystems). **B,** qRT-PCR analysis of miR-30-a,-b,-c,-d,-e and miR-30-a*, -d*, -e* expression levels in MDA-B02 and BC-M1 cells compared with MDA-MB-231 cells. Data are the mean $\pm$ SD of three to four independent experiments. Using one-way ANOVA, miR-30s expression levels in MDA-B02 and BC-M1 cells were statistically significantly different ($P <$ 0.0001) from that of MDA-MB-231 cells. **C,** qRT-PCR analysis of Dicer mRNA expression levels in MDA-B02 and BC-M1 cells, compared with MDA-MB-231 cells. Results are the mean $\pm$ SD of three independent experiments. Statistical analysis was performed using two-sided Student's t-test. **, $P <$ 0.01; ***, $P <$ 0.001.

markers N-cadherin and vimentin, whereas MDA-B02 and BC-M1 cells lost the expression of the epithelial marker E-cadherin (Supplementary Fig. S1). Of note, hierarchical clustering also showed that the expression levels of miR-30 family members were markedly downregulated in MDA-B02 and BC-M1 cells, compared with that observed in MDA-MB-231 cells (Fig. 1A).

To determine the role of the miR-30 family members in breast cancer bone metastasis, we first assessed the expression levels of miR-30s in human breast cancer cell lines by quantitative RT-PCR. The levels of each miR-30 family member, including miR-30a-5p to miR-30e-5p and miR-30a*, miR-30d*, and miR-30e* (also known as miR-30a-3p, miR-30d-3p, and miR-30e-3p), were substantially decreased in MDA-B02 and BC-M1 breast cancer cells, compared with MDA-MB-231 cells (Fig. 1B). All of the luminal [estrogen receptor (ER)-positive and/or progesterone receptor (PR)-positive] breast cancer cell lines studied (T47-D, MCF-7, BT-474, and ZR-75-1) had moderate-to-strong miR-30s expression levels, compared with basal MDA-MB-231 and MDA-B02 breast cancer cells (Supplementary Fig. S2). In basal Hs-578T cells, miR-30b and miR-30c expression levels were low, whereas expression levels of other miR-30 members were as high as in luminal breast cancer cells. miR-30 expression levels in EGF receptor2 (HER2)-positive SKBR3 cells (which are ER- and PR-negative) were high compared with that observed with HER2-positive BC-M1 cells (Supplementary Fig. S2). However, there was a general trend toward high miR-30s expression levels in ER- and/or PR-positive breast cancer cells (Supplementary Fig. S2). This was confirmed by measuring absolute amounts of miR-30s in MCF-7 and MDA-B02 cells: these amounts in MCF-7 cells were 3- to 8-fold higher than in MDA-B02 cells (Supplementary Fig. S3). Overall, these data were in line with a previous report showing that miR-30a and miR-30e are more expressed in luminal than basal breast cancer samples (38). Compared with MDA-MB-231 cells, the low miR-30 expression levels in osteotropic MDA-B02 and BC-M1 cells was explained, at least in part, by a defect in the miRNA biogenesis machinery, as exemplified by the decreased mRNA expression of Dicer (Fig. 1C), a type-III RNase involved in the processing of pre-miRNAs into mature miRNAs (6).

To determine whether miR-30s expression in tumors has a prognostic value, we analyzed by qRT-PCR the expression levels of miR-30a, miR-30b, miR-30c, miR-30d, miR-30e, and let-7c in primary tumors of 109 patients with breast cancer for whom there was no previous treatment and no evidence of distant metastasis at the time of diagnosis (35). Let-7c was used as a control for its well-known tumor suppressor role (39). Low miR-30 expression levels were significantly associated with a

tumor size ≥ 20 mm, a high grade and ER/PR-negative tumors (Supplementary Table S2). In addition, low miR-30a and miR-30e expression levels in tumors were associated with patients having positive lymph nodes. Let-7c was inversely correlated with tumor size, confirming its tumor suppressor role (39). We next calculated the univariate Cox proportional hazard regression model for distant relapse-free survival (RFS) based on expression levels of miR-30 family members (30a, 30b, 30c, 30d, and 30e) and let-7c (used here as negative control). We found that low expression levels of miR-30a, miR-30d, and miR-30e were poor prognostic factors for RFS (Supplementary Table S3). There was also a trend, although not statistically significant ($P = 0.068$), toward an association of low miR-30b expression levels with poor RFS (Supplementary Table S3). miR-30c and let-7c did not have a prognostic role for RFS ($P = 0.223$ and 0.279, respectively; Supplementary Table S3). These data collectively suggested the clinical importance of miR-30s in human breast cancer and metastasis.

miR-30s impede tumor progression and bone destruction in an experimental model of human breast cancer bone metastasis

To study the function of miR-30s in bone metastasis, ER-/PR-negative MDA-B02 cells were transduced by the retroviral vector pmiRVec containing different combinations of the five miR-30 genomic sequences downstream of a CMV promoter (see Supplementary Methods). Of note, stable overexpression of miR-30b-d or miR-30b-c in MDA-B02 cells did not modify expression levels of other members of the miR-30 family (Supplementary Fig. S4).

To determine whether miR-30s play a causal role in bone metastasis, parental MDA-B02 (MDA-B02-wt), mock-transduced MDA-B02 (MDA-B02-pmiRVec), or miR-30–over-expressing MDA-B02 cells (MDA-B02-pmiR30b-d, MDA-B02-pmiR30b-c, or MDA-B02-pmiR30a-b-c-d-e) were injected into the tail artery of immunodeficient mice. Using this animal model, radiographic analysis on day 32 after tumor cell injection revealed that the extent of osteolytic lesions in animals bearing MDA-B02-pmiR30a-b-c-d-e tumors was 2- to 2.5-fold lower than that of animals bearing pmiRVec- or MDA-B02-wt-tumors (Table 1; Fig. 2A). Bioluminescence imaging indicated that there was also a reduction of tumor burden in hind limbs of animals bearing MDA-B02-pmiR-30a-b-c-d-e tumors, compared with that observed with MDA-B02-wt and MDA-B02-pmiRVec tumor-bearing animals (Fig. 2B). Histomorphometric analysis of hind limbs with metastases from animals bearing miR-30s tumors showed that the BV/TV ratio (a measure of the bone volume) was substantially increased, compared with pmiRVec-tumor-bearing animals (Table 1; Fig. 2C). This

Table 1. miR30 overexpression in MDA-B02 breast cancer cells decreases cancer-induced osteolytic lesions in animals

| Cell line | Radiography | | Histomorphometry | | | | TRAP staining | |
	mm²/mouse	P	BV/TV (%)	P	TuV/STV (%)	P	OC.S/BS (%)	P
MDA-B02-wt	13 ± 1.1 (n = 8)	ns						
MDA-B02-pmirVec	14.1 ± 1.7 (n = 10)	—	11.9 ± 2.4 (n = 13)	—	45.2 ± 5.4 (n = 13)	—	77.4 ± 8.1 (n = 5)	—
MDA-B02-pmir-30b-d	7.7 ± 1.2 (n = 9)	0.01	20.9 ± 5.3 (n = 5)	0.01	14.7 ± 5.6 (n = 5)	0.02	60.3 ± 2.2 (n = 5)	0.05
MDA-B02-pmir-30b-c	6 ± 0.96 (n = 7)	0.01	27.6 ± 2.7 (n = 5)	0.01	24.7 ± 2.5 (n = 5)	0.02	48 ± 1.5 (n = 4)	0.01
MDA-B02-pmir30a-b-c-d-e	5.7 ± 0.8 (n = 6)	0.02	26.6 ± 2.7 (n = 4)	0.02	21.8 ± 6.1 (n = 4)	0.05	41.7 ± 16.5 (n = 4)	0.02

NOTE: All measurements were made 32 days after tumor cell inoculation. P values (two-sided) are for pairwise comparisons with MDA-B02-pmirVec control group using the Mann–Whitney U test.
Abbreviations: BV/TV, bone volume-to-tissue volume ratio; TuV/STV, tumor volume-to-soft tissue volume ratio; TRAP, tartrate-resistant acid phosphatase; OC.S/BS, active osteoclast resorption surface-to-bone surface; ns, nonsignificant; —, not applicable (referent).
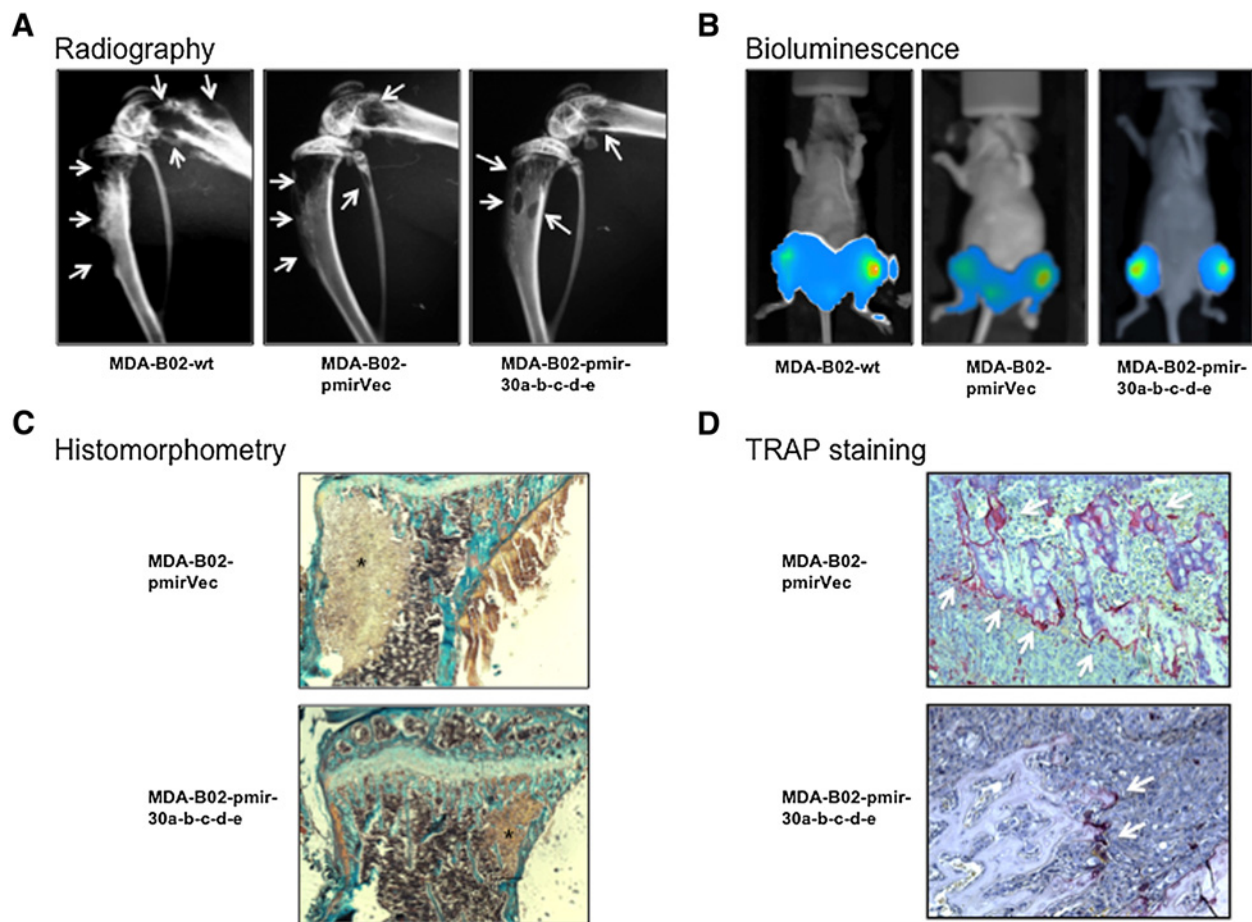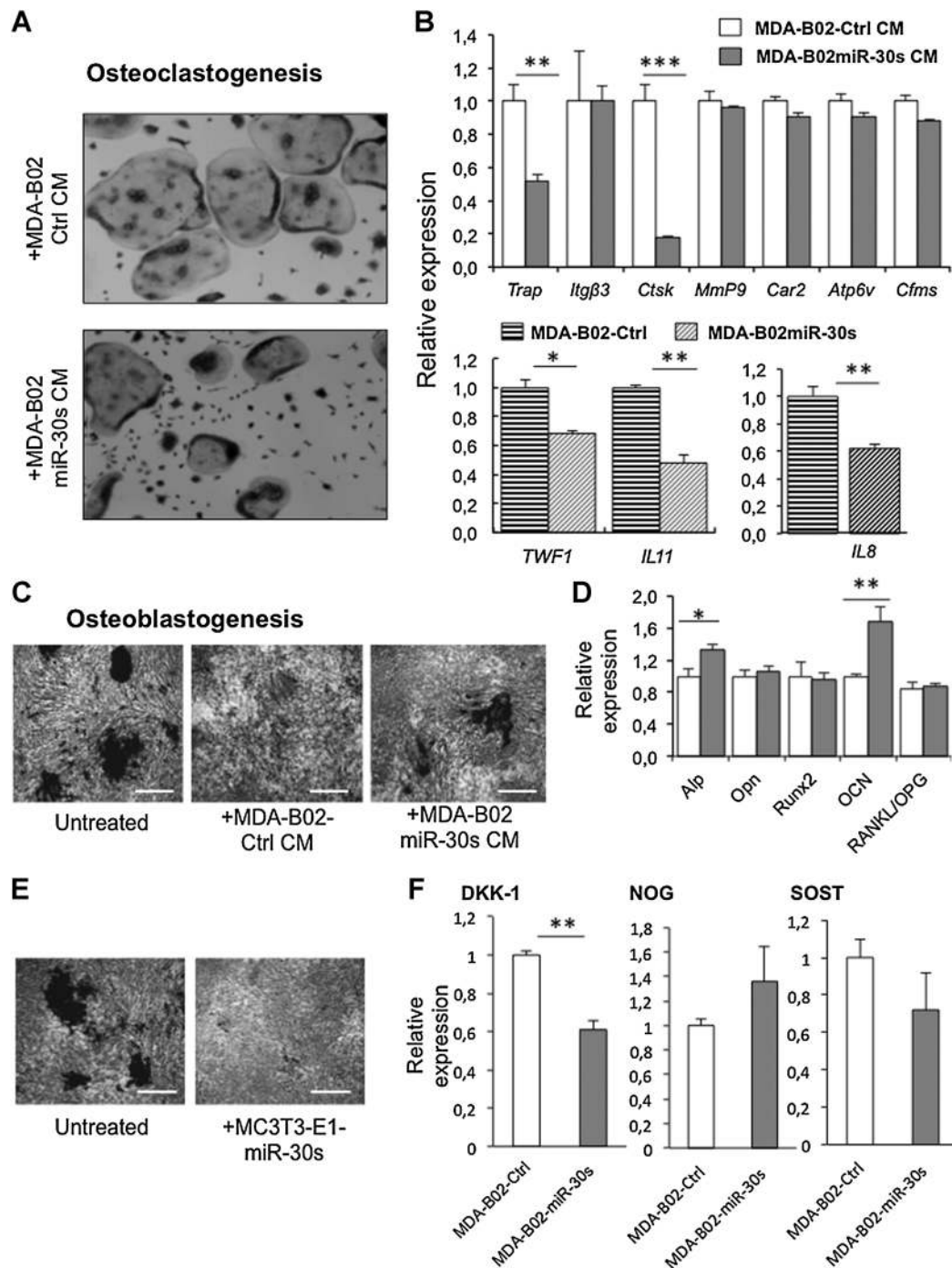
Figure 2.
miR-30s overexpression in breast cancer cells reduces the extent of osteolytic lesions and skeletal tumor burden in metastatic animals. **A,** Representative radiographs of hind limbs with osteolytic lesions (arrows) from female Balb/c *nude* mice bearing breast tumors at day 32 after tumor cell inoculation. MDA-B02-wt, parental cells; MDA-B02-pmiRVec, mock-transfected cells; MDA-B02-pmiR-30a-b-c-d-e, miR30s-overexpressing cells. **B,** Representative whole body bioluminescence imaging of animals bearing MDA-B02-wt, MDA-B02-pmiRVec, or MDA-B02-pmiR30a-b-c-d-e tumors at day 32 after tumor cell inoculation. **C,** Goldner trichrome staining of tissue sections of tibial metaphysis from tumor-bearing animals. Bone is stained green, whereas bone marrow is stained violet and tumor cells (asterisk) are stained brown. **D,** TRAP-stained metastatic bone tissue sections. Osteoclasts on bone surfaces are stained red (white arrows). The images shown are examples that best illustrate miR-30s' effects on inhibition of bone destruction and tumor burden.

difference was accompanied by a sharp reduction in the TuV/ STV ratio (a measure of the skeletal tumor burden) in miR-30s tumor-bearing animals, compared with pmiRVec-tumor-bearing animals (Table 1; Fig. 2C). In addition, there was a decrease in the TRAP staining of bone tissue sections of metastatic legs from miR-30s tumor-bearing animals (indicating a decrease of active-osteoclast resorption surfaces), compared with pmiRVec-tumor-bearing animals (Table 1; Fig. 2D). Similar results were obtained with MDA-B02 cells overexpressing miR-30b-d or miR-30b-c (Table 1). Overall, these data indicated that miR-30s inhibit breast cancer bone metastasis.

miR-30s restore the balance between bone resorption and bone formation

Tumor cells promote bone destruction through the production of factors that stimulate osteoclast formation and repress osteoblast formation, resulting in an imbalance between bone resorption and bone formation (1, 3). After having observed that miR-

30s overexpression in MDA-B02 cells inhibited bone destruction in animals (Table 1; Fig. 2), we then asked whether miR-30s had any influence on osteoclast differentiation. We treated primary mouse bone marrow cell cultures with RANKL and M-CSF together with the conditioned medium from MDA-B02 cells transfected with a mix of the five miR-30s-5p mimics at equimolar concentrations (MDA-B02-miR-30s) or by equivalent concentrations of a negative control miR scramble sequence (MDA-B02-Ctrl). Consistent with *in vivo* data (Fig. 2D; Table 1), the conditioned medium from MDA-B02-miR-30s cells decreased the formation of TRAP-positive multinucleated osteoclasts, compared with that of MDA-B02-Ctrl cells (316 ± 29 vs. 416 ± 8 osteoclasts/well; $n = 3$; $P < 0.001$; Fig. 3A). This inhibitory effect of the conditioned medium from MDA-B02-miR-30 cells on osteoclastogenesis was accompanied by a decreased expression of *Trap* (a marker associated with osteoclast differentiation) and *Ctsk* (an osteoclast-derived cysteine protease enabling degradation of the collagenous matrix) in osteoclasts (Fig. 3B). The expression levels of other

Figure 3.
miR-30s restore bone homeostasis. **A,** *In vitro* osteoclast differentiation of murine bone marrow cells treated with M-CSF+RANKL in combination with the conditioned medium (CM) of mock-transfected MDA-B02 cells (MDA-B02-Ctrl) or MDA-B02 cells overexpressing miR-30s (MDA-B02-miR-30s). Mature osteoclasts were quantified as multinucleated (more than three nuclei), TRAP-positive cells. Representative images are shown for each group. **B,** Top graphs: RT-qPCR analysis of murine osteoclasts treated with the conditioned medium from MDA-B02-Ctrl or MDA-B02-miR-30s cells. *Atp6v*, V-ATPase; *Car2*, anhydrase carbonic; *Cfms*, colony-stimulating factor-1 receptor; *Ctsk*, cathepsin K; *Itgb3*, integrin beta-3; *Mmp9*, matrix metalloprotease 9; *Trap*, tartrate-resistant acid phosphatase. Bottom graphs, RT-qPCR analysis of MDA-B02-Ctrl and MDA-B02-miR-30s cells. *TWF1*, twinfilin-1. **C,** *In vitro* differentiation of osteoblastic MC3T3-E1 cells cultured in osteogenic conditions with or without conditioned medium from MDA-B02-Ctrl or MDA-B02-miR-30s cells. Bone mineralized nodules stain black with von Kossa staining. **D,** RT-qPCR analysis of MC3T3-E1 cells treated with the conditioned medium from MDA-B02-Ctrl or MDA-B02-miR-30s cells. Alp, alkaline phosphatase; Ocn, osteocalcin; Opg, osteoprotegerin; Opn, osteopontin; Rankl, receptor activator of nuclear factor kappa-B ligand; Runx2, Runt-related transcription factor 2. **E,** *In vitro* differentiation of MC3T3-E1 cells cultured in osteogenic conditions, then left untreated or transfected with miR-30s mimics. **F,** RT-qPCR analysis of MC3T3-E1 cells treated with the conditioned medium from MDA-B02-Ctrl or MDA-B02-miR-30s cells. Dkk-1, Dickkopf-related protein 1; Nog, noggin; Sost, sclerostin. For qRT-PCR analyses, data are the mean ± SD of three separate experiments. *P* values (two-sided) are for pairwise comparisons with the control group using the Mann–Whitney *U* test (*, $P < 0.05$; **, $P < 0.02$; ***, $P < 0.01$).

markers associated with osteoclast differentiation (e.g., *Car2*, *Cfms*, *ATP6v*) and cytoskeleton morphology (e.g., *Itgb3*) were not affected (Fig. 3B). MDA-B02 cells secrete cytokines and interleukins known to stimulate osteoclast activity (IL8, IL11, MCP-1; ref. 36). Compared with MDA-B02-Ctrl cells, miR-30 overexpression in MDA-B02 cells inhibited *IL8*, *IL11*, and *TWF1* (twinfilin1), an upstream regulator of *IL11* expression (Fig. 3B; ref. 26). In addition, the inhibitory effect of miR-30s on *IL8* and *IL11* expression was validated by ELISA, demonstrating a reduced production of these ILs in the conditioned medium of MDA-B02-miR-30 cells, compared with that of MDA-B02-Ctrl cells (193 ± 80 vs. 375 ± 70 pg/mL and 345 ± 219 vs. 821 ± 345 pg/mL, respectively; $n = 3$; $P < 0.05$).

We next investigated whether miR-30s expression in MDA-MB-B02 cells could also influence osteoblastogenesis (Fig. 3C). The conditioned medium from MDA-B02-Ctrl cells inhibited the formation of bone nodules and their mineralization, compared with untreated osteoblasts (Fig. 3C). In contrast, the conditioned medium from MDA-B02-miR-30s cells significantly reversed the inhibitory effect on osteoblast differentiation (Fig. 3C) and increased the expression of markers associated with osteoblast differentiation (*Alp*, *Ocn*; Fig. 3D). Interestingly, however, the direct transfection of MC3T3-E1 osteoblasts with the five miR-30 mimics at equimolar concentrations induced a strong inhibition of osteoblastogenesis (Fig. 3E). These findings were in agreement with a previous study (16) showing that miR-30s negatively regulate osteoblast differentiation. Thus, our results demonstrated that miR-30 mimics used to transfect MDA-B02 cells were not secondarily released into the conditioned medium of transfected cells. Osteoblast differentiation would have been otherwise inhibited. Instead, miR-30 mimics mediated translational repression of specific mRNAs, which was followed by a decreased secretion of proteins by MDA-B02-miR-30s cells that, in turn, negatively regulated osteoblastogenesis. In this respect, we found that miR-30 mimics inhibited *DKK-1* in MDA-B02 cells, whereas the expression of other osteoblast differentiation inhibitors (*NOG*, *SOST*) remained unaffected (Fig. 3F).

Collectively, the above data indicate that miR-30s act in tumor cells by decreasing the production of osteoclast differentiation stimulators (IL8, IL11) and osteoblast differentiation inhibitors (DKK-1), which, in turn, partially restore the balance between bone resorption and bone formation, leading to a reduction of bone destruction *in vivo*.

miR-30s reduce primary breast cancer outgrowth *in vivo* by inhibiting tumor cell invasion

We observed that miR-30 overexpression reduces bone destruction and skeletal tumor burden in animals (Fig. 2; Table 1). As bone is resorbed, bone-derived growth factors that are stored in the bone matrix are released and stimulate tumor growth (1, 3). To be free from the impact of growth factors released from resorbed bone that stimulate skeletal tumor outgrowth, we investigated the role of miR-30s in breast cancer cell growth using *in vivo* experiments in which MDA-B02 cells overexpressing miR-30b and -30d (MDA-B02-pmiR30b-d) and their control counterparts (MDA-B02-pmiRVec) were implanted subcutaneously in animals. Tumor outgrowth did not differ between groups until day 35 after tumor cell inoculation, indicating that miR-30b and -30d did not interfere with tumor take. However, MDA-B02-pmiR30b-d tumors grew more slowly afterwards, resulting in a significantly

lower tumor volume at day 50 after tumor cell inoculation, compared with MDA-B02-pmiRVec tumors (Fig. 4A). Immunostaining of tumor xenografts with an anti-CD31 antibody that specifically recognizes murine endothelial cells showed that miR30b-d overexpression was associated with decreased vascularization of MDA-B02-pmiR30b-d tumors compared with MDA-B02-pmiRVec tumors (Fig. 4B). The proliferative index of MDA-B02-pmiR30b-d tumors, as judged by Ki67 immunostaining, was also decreased compared with MDA-B02-pmiRVec tumors (Fig. 4C). However, miR30b-d overexpression or the use of synthetic miR-30 mimics did not affect MDA-B02 cell proliferation *in vitro* (Fig. 4D and E). In contrast, MDA-B02 cell invasion was similarly negatively affected by the stable overexpression of miR-30b-d, miR-30b-c, or miR-30a-b-c-d-e (Fig. 4F). In addition, the treatment with antagomiRs of MDA-B02 cells stably transduced with the different genomic sequences of miR-30s restored the invasiveness properties of these cells (Fig. 4G). The transfection of MDA-B02 or BCM-1 cells with equimolar concentrations of miR-30 mimics (miR-30a-b-c-d-e) also inhibited tumor cell invasion compared with their respective control counterparts (Fig. 4H). Thus, these data indicate that miR-30s inhibit breast cancer cell invasion, providing an explanation for tumor growth reduction.

miR-30s directly target multiple genes associated with bone metastasis formation, including targets such as *CDH11*, *ITGA5*, and *ITGB3*

To identify direct miR-30 target mRNAs, we first used a publicly available miRNA target prediction program (Targetscan) and then performed experimental validation analyses. The online target gene prediction analysis allowed us to identify 3′-UTR putative direct binding sites for miR-30s that we then narrowed to 53 genes on the basis of their involvement in signaling pathways associated with bone metastasis (Supplementary Table S4). Among these, we identified the transcription factor RUNX2, which was previously reported to be a direct target for mir-30c (17). Besides *RUNX2*, we found that miR-30s reduced the expression of several other osteomimetic genes (*CDH11*, *CX43*, *DKK1*) in MDA-B02 and BC-M1 breast cancer cells (Supplementary Fig. S5). As aforementioned, miR-30s also inhibited the expression of genes associated with osteoclastogenesis, such as *IL8*, *IL11*, and *TWF1* (twinfilin1), an upstream regulator of *IL11* expression (Fig. 3B; Supplementary Fig. S5; ref. 26). They also inhibited the expression of integrins (*ITGA5*, *ITGB3*) and connective tissue growth factor (*CTGF*; Supplementary Fig. S5). Of note, we confirmed by Western blotting analysis that there was a moderate-to-strong inhibition of the expression of these miR-30 targets at the protein level (Supplementary Fig. S6).

We then focused our attention to *CDH11*. Interestingly, as opposed to the majority of genes for which miR-30s bind to the 3′-UTR of target mRNAs, the miRNA:mRNA alignment analysis showed that a conserved 8-mer site in the open reading frame (ORF) of *CDH11* matched the seed region of the five miR-30 family members (Supplementary Fig. S7). The homology test showed that this binding site for miR-30s was evolutionary conserved among various vertebral species and that the thermodynamic stability of the base pairing duplexes was compatible with efficient inhibition of *CDH11* expression (Supplementary Fig. S7). In agreement with these observations, there was a stark reduction of CDH11 protein levels in
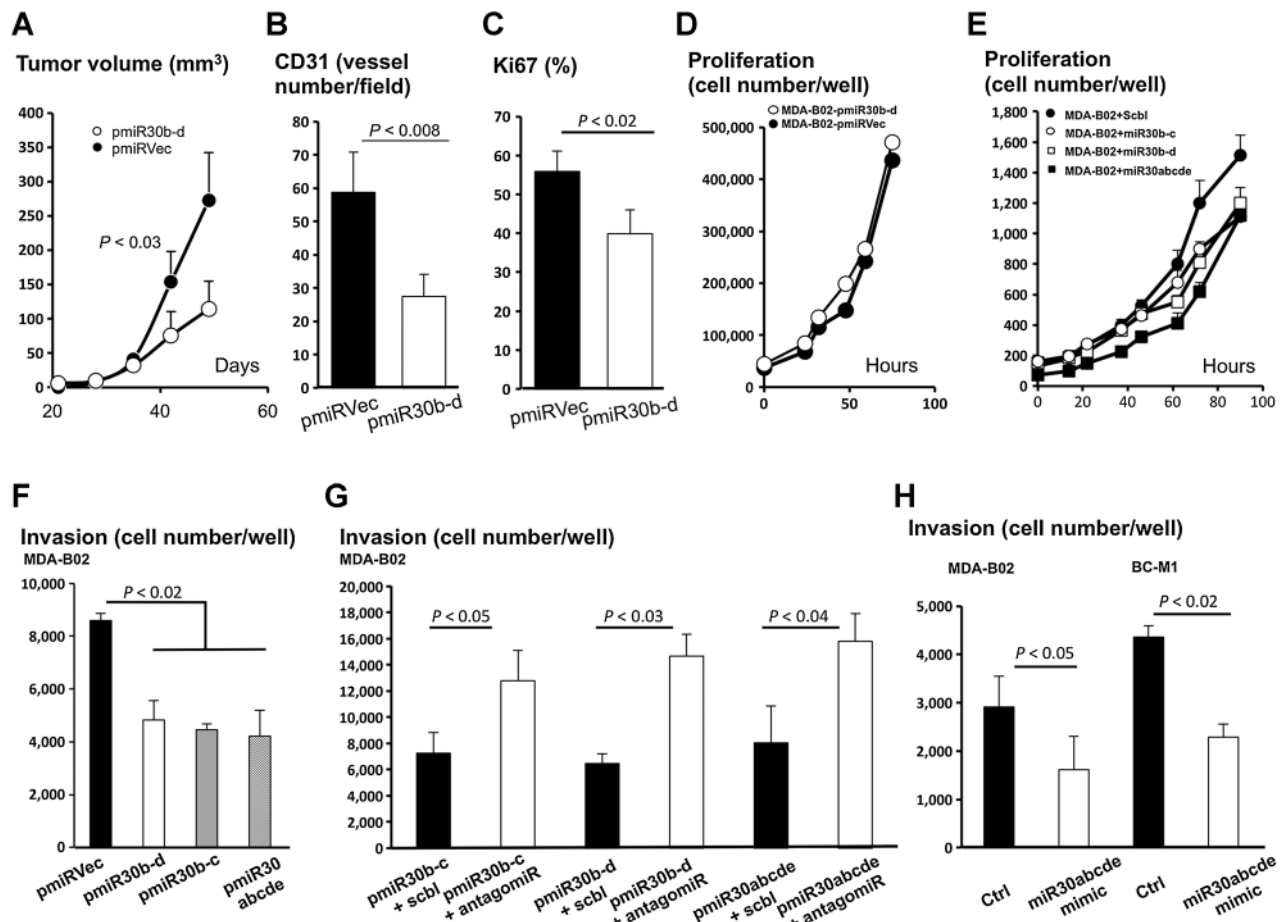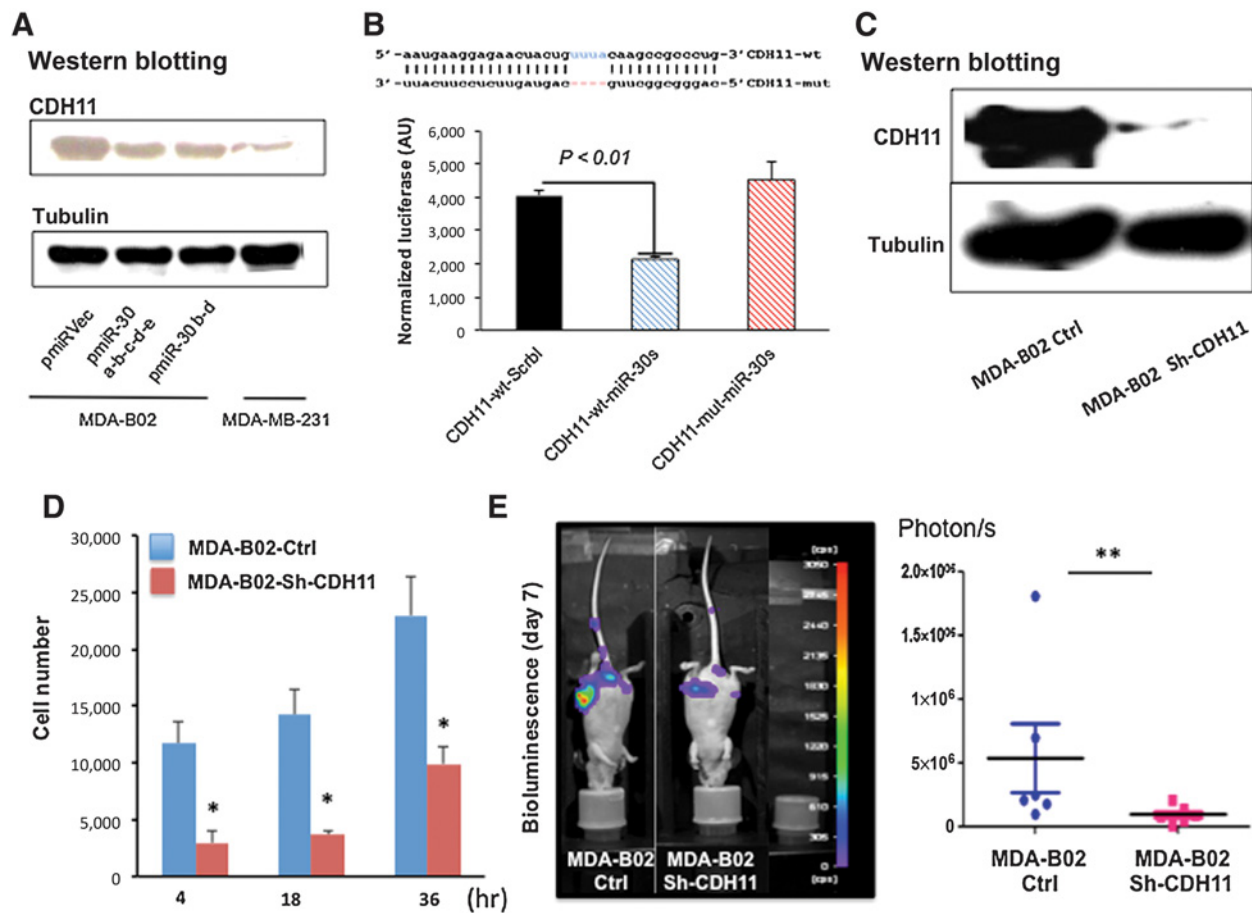
Figure 4.

miR-30s reduce breast cancer outgrowth *in vivo* and tumor cell invasion *in vitro*. **A,** MDA-B02-pmiRVec (control) and MDA-B02-pmiR-30b-d cells were inoculated subcutaneously in female *Balbc* nude mice. Tumor volumes were measured with a Vernier caliper. **B** and **C,** CD31 and Ki-67 immunostaining of tissue sections of harvested tumors from mice inoculated with MDA-B02-pmiRVec and MDA-B02-pmiR-30b-d, as a measurement of the number of tumor-associated blood vessels and proliferative index of tumor cells, respectively. **D,** Counting of MDA-B02-pmiRVec and MDA-B02-pmiR-30b-d cells in culture as a function of time after cell plating. **E,** MDA-B02 cells were transfected with miRNA mimics (30-b and- c, 10 nmol/L each; 30-d and-b, 10 nmol/L each; 30abcde, 10 nmol/L each) or scramble mimics (Scbl; 50 nmol/L). Transfected cells in culture were enumerated as a function of time, 48 hours after cell plating. **F,** MDA-B02-pmiRVec, MDA-B02-pmiR-30b-d, MDA-B02-pmiR-30b-c, and MDA-B02-pmiR-30abcde cells were loaded in inserts with a porous membrane coated with basement membrane Matrigel (top chamber), and the chemoattractant (serum) was placed in wells of the companion plate (bottom chamber). After 24-hour incubation at 37°C, the noninvading cells were removed and the invading cells on the under surface of the inserts were fixed, stained, and counted under microscope. **G,** Same as in **F** for MDA-B02 cells transduced with different genomic sequences of miR-30s and treated with their corresponding antagomiR-30s or a scramble antagomiR (negative control). Results were obtained after 48-hour incubation at 37°C. **H,** Same as in **F** for MDA-B02 and BC-M1 cells transfected with equimolar concentrations (10 nmol/L) of each miR-30 mimic or with 50 nmol/L of scramble mimic (negative control). *In vivo* and *in vitro* data are the mean ± SD of three separate experiments. *P* values (two-sided) are for pairwise comparisons with control group using unpaired Student *t* test.

MDA-B02 cells transfected with miR-30s, compared with MDA-B02-ctrl cells (Fig. 5A). To validate a direct targeting of *CDH11* by miR-30s, HEK-293T cells overexpressing or not overexpressing miR-30s were transiently transfected with the psiCHECK-2 vector, in which was cloned the ORF of *CDH11* containing the wild-type or mutated conserved binding site for miR-30s. As shown in Fig. 5B, luciferase expression only decreased when HEK-293T cells overexpressing miR-30s were transfected with wild-type ORF-*CDH11* vector, indicating that the 8-mer binding site for miR-30s in the ORF of *CDH11* was functional. Similarly, following transient transfection of MDA-B02-ctrl, MDA-B02-pmiR-30a-b-c-d-e and MDA-MB-231 cells with the psiCHECK-2-ORF-CDH11 vector, luciferase expression was

only reduced in tumor cells overexpressing miR-30s (Supplementary Fig. S7). Thus, *CDH11* is a direct target for repression by miR-30s. To further validate the role of CDH11, we then examined whether the silencing of *CDH11* expression in MDA-B02 cells would repeat the inhibitory effect of miR-30s on bone metastasis formation. Compared with MDA-B02 control cells, cadherin-11 protein expression levels in MDA-B02-shCDH11 cells were reduced by >90% as analyzed by Western blotting (Fig. 5C). In addition, as previously reported for prostate cancer cell interaction with osteoblasts (40), the silencing of *CDH11* in luciferase-expressing MDA-MB-231, MDA-B02 and Hs578T cells also decreased breast cancer cell interaction to osteoblasts (Fig. 5D; Supplementary Fig. S8). Moreover, *CDH11* silencing

Figure 5.
Cadherin-11 (CDH11) is a direct target for repression by miR-30s. **A,** Western blotting of CDH11 and α-tubulin in MDA-B02 cells transduced with different genomic sequences of miR-30s, compared with parental MDA-MB-231 cells. Tubulin was used as a control for equal loading. **B,** Relative luciferase activity in HEK-293T cells overexpressing miR-30s (CDH11-wt-miR-30s and CDH11-mut-miR-30s) or not overexpressing miR-30s (CDH11-wt) that were transiently transfected with psiCheck2-CDH11 reporter vector containing either the wild-type (CDH11-wt, CDH11-wt-miR-30s) or mutated (CDH11-mut-miR-30s) binding site. Values are normalized to that of the internal firefly luciferase. Mean ± SD; $n = 3$. **C,** Western blotting of CDH11 and α-tubulin in parental MDA-B02 cells and MDA-B02 cells silenced for CDH11 (MDA-B02-sh-CDH11). **D,** MDA-B02 and MDA-B02-sh-CDH11 cell interaction with MC3T3-E1 osteoblasts as a function of time after cell plating. Mean ± SD; $n = 3$. **E,** CDH11 silencing in MDA-B02 reduced bone metastasis burden *in vivo*. Bioluminescence was analyzed in mice inoculated intra-arterially with MDA-B02-Ctrl and MDA-B02-Sh-CDH11 cells ($n = 6$ per group), 7 days after tumor cell injection. For *in vitro* and *in vivo* experiments, P values (two-sided) are for pairwise comparisons with control group using the MannWhitney U test (*, $P < 0.05$; **, $P < 0.02$).

in MDA-B02 cells drastically reduced bone metastasis burden *in vivo* (Fig. 5E).

Strikingly, a strong over-representation of genes associated with tumor cell adhesion and invasion (e.g., integrins α2β1, α5β1, α4β1 and αvβ3, connective tissue growth factor) was also observed among miR-30 downregulated genes (Supplementary Table S4). We found a conserved 8-mer binding site in the 3′UTR of integrin β3 (*ITGB3*) and of *CTGF* that matched with the seeding region of the five miR-30 family members (Supplementary Fig. S9). CTGF enhances the motility of breast cancer cells via an integrin-αvβ3-dependent signaling pathway (41). In accordance with these results, *CTGF* was poorly expressed in MDA-MB-231 that contain high endogenous levels of levels of miR-30s and we observed a marked reduction of *CTGF* and *ITGB3* expression in MDA-B02 cells stably transfected with the retroviral vector pmiR-Vec containing the five miR-30s (Supplementary Fig. S9). To validate the direct targeting of *CTGF* by miR-30s, HEK-293T cells

overexpressing or not overexpressing miR-30s were transiently transfected with the luciferase reporter psiCHECK-2 vector, in which was cloned the 3′UTR of *CTGF* containing either the wild-type or mutated sequence of the conserved binding site for miR-30s. As shown in Supplementary Fig. S9, miR-30s significantly decreased relative luciferase activity in HEK-293T cells overexpressing miR-30s compared with their control counterparts. In contrast, luciferase activity was not decreased when HEK-293T cells overexpressing miR-30s were transfected with mutated 3′UTR *CTGF* vector (Supplementary Fig. S9), indicating that the 8-mer binding site was functional.

Among putative integrin targets for miR-30s (supplementary Table S4), *ITGA5* was identified as being a novel direct target for repression by miR-30s. The miRNA:mRNA alignment analysis showed that a conserved 8-mer site in the 3′UTR of *ITGA5* matched the seed region of the five miR-30 family members (Supplementary Fig. S10). Transient transfection of HEK-293T

Figure 6.
ITGA5 is a direct target for repression by miR-30s. **A,** Relative luciferase activity in HEK-293T cells expressing miR-30s mimics (ITGA5-wt-miR30s, ITGA5-mut-miR-30s) or a scramble mimic (ITGA5-wt-Scrbl) that were cotransfected with the psiCheck2-ITGA5 reporter vector containing either the wild-type (ITGA5-wt-Scrbl, ITGA5-wt-miR30s) or mutated (ITGA5-mut-miR-30s) binding site. Values are normalized to that of the internal firefly luciferase. Mean ± SD; $n = 3$. **B,** Western blotting of ITGA5 and α-tubulin in MDA-B02 and BC-M1 cells after cell transfection with negative control scramble mimics (Ctrl) or miR-30s mimics (miR-30s). Tubulin was used as a control for equal loading. **C,** Western blotting for ITGA5 expression in mock-transduced (Scrbl) and ITGA5-silenced Hs-578T breast cancer cells (ITGA5-silenced). Tubulin was used as a control for equal loading. **D,** Left, whole body bioluminescence imaging of animals at day 7 after intra-arterial inoculation of luciferase expressing Hs-578T cells that were previously mock-transduced or silenced for ITGA5 expression. Right, graphs showing the percentage of metastatic animals in each group (5–8 animals per group). $P < 0.00001$; P value (two-sided) is for pairwise comparison with mock-transduced cells using the Mann–Whitney U test. **E,** Bone metastasis suppression by multiple miR-30 regulatory networks. miR-30s repress genes that are associated with osteomimicry, invasion, and bone destruction, thereby inhibiting bone metastasis formation. CDH11, cadherin-11; CTGF, connective tissue growth factor; Dkk-1, Dickkopf-related protein 1; ITGA5, integrin alpha5; ITGB3, integrin beta3; Runx2, Runt-related transcription factor 2.

cells overexpressing miR-30s with the psiCHECK-2-wild-type 3′UTR-*ITGA5* vector led to a decrease in luciferase activity, whereas transfection with the mutated 3′UTR-*ITGA5* vector had no inhibitory effect (Fig. 6A). Thus, the 8-mer binding site for miR-30s in the 3′UTR of *ITGA5* was functional. In addition, transfection of MDA-B02 and BC-M1 cells with miR-30 mimics caused a moderate-to-strong reduction of ITGA5 protein levels (Fig. 6B). To further validate the role of ITGA5, we then examined whether the silencing of *ITGA5* expression in Hs-578T cells (a triple-negative breast cancer cell line expressing high *ITGA5* levels) would recapitulate the inhibitory effect of miR-30s on bone metastasis formation. Compared with Hs-578Tluc2 control cells, ITGA5 protein expression levels were drastically reduced in *ITGA5*-silenced Hs-578Tluc2 cells as analyzed by Western blotting (Fig. 6C). Moreover, the silencing of *ITGA5* in luciferase-expressing Hs-578Tcells led to a substantial reduction of bone metastasis burden *in vivo* (Fig. 6D).

Discussion

Our study establishes that miR-30 family members (miR-30a, miR-30b, miR-30c, miR-30d, and miR-30e) act as tumor suppressor genes in breast cancer bone metastasis. Specifically, we showed that miR-30s reduce breast cancer cell invasion, osteomimicry and bone destruction *in vivo* by targeting multiple bone metastasis-associated genes, including *CTGF*, *ITGB3*, *ITGA5*, *IL8*, *TWIF1/IL11*, *DKK-1*, *RUNX2*, and *CDH11* (Fig. 6E). This inhibitory effect of miR-30s on breast cancer bone metastasis formation was the same, whether tumor cells overexpressed miR-30b/d, miR-30b/c or the whole miR-30 family. Although miR-30 family members express different 3′ complementary sequences (16), they all share the same 5′ seed sequence and, therefore, act through common targets to reduce skeletal tumor burden and block tumor-driven osteolytic lesions. Similarly, Zhang and colleagues reported that there is no additive effect of the whole family of miR-30s on inhibition of metadherin (*MTH*) expression

in human breast cancer cells, compared with miR-30a alone (22). The reason behind overexpressing pairs of some miR-30 family members was to investigate specific traits of miR-30 biology. During miRNA biogenesis, pre-miRNAs are exported in the cytoplasm as miRNA:miRNA* duplexes, which are processed by Dicer and then they associate with Argonaute proteins to form a complex (42). Only the mature miRNA (miRNA-5p) is retained in the complex, while the other strand of the duplex (miRNA* or miRNA-3p) is degraded (42). However, miRNA-3ps can be thermodynamically stable and bind to mRNAs, suggesting they could play a cooperative role with miRNA-5ps by targeting the same mRNA (43). In our study, we showed that MDA-MB-231, MDA-B02 and BC-M1 cells expressed both strands for miR-30a, miR-30d and miR-30e, whereas only the mature miRNA-5p was expressed for miR-30b and miR-30c (Fig. 1B). The reduction of bone metastasis burden in vivo was however the same whether MDA-B02 cells overexpressed miR-30b/c or miR-30-a-b-c-d-e (Table 1), thereby indicating that only the mature miRNA-5p strands of miR-30s were responsible for inhibition of bone metastasis. The inhibitory effect of miR-30b and miR-30c would have been otherwise lower than that of miR-30-a-b-c-d-e. We overexpressed miR-30b and miR-30d in breast cancer cells because this pair of genes is in cluster on the same chromosome (16). We surmised that they might be coordinately involved in the regulation of bone metastasis formation. Overexpression of miR-30b/d did not, however, function more efficiently than miR-30b/c and miR-30-a-b-c-d-e to inhibit osteolysis (Table 1). Overall, our results are in line with previous experimental findings showing that miR-30 family members suppress primary tumor growth and soft tissue metastasis (lung, liver) in different animal models of cancer (breast, colon, liver, osteosarcoma, thyroid; refs. 19–27, 31). However, to the best of our knowledge, this is the first time the contribution of miR-30 family members in bone metastasis is reported.

Breast cancer cells promote bone destruction through the production of factors that stimulate osteoclast formation (e.g., IL8, IL11, MCP-1) and repress osteoblast formation (e.g., DKK-1, SOST, noggin), resulting in an imbalance between bone resorption and bone formation (1, 3, 36). Here, we show that miR-30s inhibited the expression of osteoclast differentiation stimulators IL8 and IL11 and reduced their protein levels. In addition, the expression of TWF1, an upstream regulator of IL11, was inhibited, which was in agreement with a previous finding (26) showing that miR-30c suppresses IL11 expression through inhibition of TWF1. Other miRNAs (miR-204, miR-211, and miR-379), whose expression is downregulated in highly MDA-MB-231 bone metastatic variants, have been identified as potent inhibitors of TGFβ-induced IL11 secretion (17). Beside inhibition of bone resorption, we show that miR-30s reduced the expression of the osteoblast differentiation inhibitor DKK-1 in breast cancer cells. SOST is another osteoblast differentiation inhibitor in breast cancer cells whose expression is inhibited by miR-218 (44). Collectively, these data indicate that miR-30s, as well as other miRNAs (miR-204, miR-211, miR-218, and miR-379), are capable of restoring bone homeostasis, thereby impairing breast cancer–induced bone destruction in vivo.

Tumor cells can adapt to the bone microenvironment by expressing genes that are normally expressed by osteoblasts and osteoclasts (10, 14, 15, 36). Here we focused our attention on CDH11 because (i) it is the archetype of osteoblast differentiation,

and (ii) previous studies have revealed its crucial role in breast and prostate cancer bone metastasis formation by promoting tumor cell invasion and interactions with osteoblasts (40, 45, 46). We found that CDH11 is a novel direct target for repression by miR-30s. Moreover, CDH11 silencing in breast cancer cells recapitulated inhibitory effects of miR-30s on skeletal tumor burden in vivo (Fig. 5). Interestingly, miR-30s bound directly in the coding region of CDH11. It has been proposed that the direct targeting of miRNAs to the coding region may speed up the silencing of stable mRNAs (47). Other miRNAs (miR-135, miR-203, and miR-218) have been reported to inhibit SOST and RUNX2 expression in breast cancer cells, which are two other osteoblastic genes associated with tumor cell osteomimicry (44, 48). Thus, the dysregulation of miR-30s and other microRNAs (miR-135, miR-203, miR-218) in breast cancer cells enhances abnormal expression of osteoblast-specific genes (CDH-11, RUNX2, DKK-1, SOST), which endows tumor cells with full competence for outgrowth in the bone marrow.

Among genes that are downregulated by miR-30s, we observed a strong overrepresentation of genes associated with tumor cell adhesion and invasion. Of note, ITGA5 was identified as a novel direct target for repression by miR-30s. ITGA5 mediates breast cancer cell adhesion and migration, which results in lymph node and lung metastasis formation in animal models (49, 50). ITGA5 has been also identified as a transcriptional target of RUNX2 (51). Its role in bone metastasis formation was, however, unknown. Here, we show that the silencing of ITGA5 in triple-negative breast cancer cells recapitulated the inhibitory effect of miR-30s on bone metastasis formation in vivo, suggesting that this integrin could be an interesting target for therapeutic intervention in bone metastasis. This hypothesis clearly warrants further investigation. Two additional genes, CTGF and ITGB3, which are involved in bone metastasis formation, were also identified as direct miR-30 targets. CTGF is a proinvasive and angiogenic factor that enhances the motility of breast cancer cells via an ITGB3-dependent signaling pathway and it promotes the formation of osteolytic lesions in animals (3, 41, 52). ITGB3 confers on breast cancer cells a greater propensity to metastasize to bone (32, 53). We found conserved binding sites in the 3'UTR of CTGF and ITGB3 that matched with the seeding region of the five miR-30 family members. These findings were in agreement with previous reports showing that CTGF and ITGB3 are direct targets for miR-30a and miR-30c in colorectal cancer cells and cardiomyocytes, respectively (17, 54). In addition, miR-30a inhibits invasiveness of breast and colorectal cancer cells in vitro (17, 22), which is in agreement with our study.

The main limitation of our study is that experimental bone metastases were conducted using triple-negative breast cancer cells, whereas ER-positive breast cancers are prone to metastasize to bone. All of the ER-positive breast cancer cell lines studied (T47D, MCF-7, BT-474, and ZR-75-1) had moderate-to-high miR-30s expression levels, compared with triple-negative MDA-B02 and BC-M1 breast cancer cells (Supplementary Figs. S2 and S3). In an attempt to better reflect bone metastasis from human breast cancer, we therefore transfected ER-positive MCF-7 cells with antagomiR-30s to induce a functional blockade of miR-30s. However, antagomiR-30s did not modulate MCF-7 cell migration and invasion in vitro and did not interfere with MCF-7 cell bone marrow colonization in vivo (Supplementary Fig. S11). Thus, our results only apply to triple-negative breast cancer.

In conclusion, our findings show that miR-30s employ multiple mechanisms to impede breast cancer bone metastasis, reducing tumor cell invasion, osteomimicry, and bone destruction *in vivo* by directly targeting multiple genes. Some of these genes may represent attractive targets for developing new therapeutic strategies in the management of bone metastasis associated with triple-negative breast cancer.

Disclosure of Potential Conflicts of Interest

No potential conflicts of interest were disclosed.

Authors' Contributions

Conception and design: M. Croset, F. Pantano, K. Pantel, P. Clézardin
Development of methodology: M. Croset, N. Allioli
Acquisition of data (provided animals, acquired and managed patients, provided facilities, etc.): M. Croset, F. Pantano, E. Bonnelye, F. Descotes, R. Bachelier, S.-S. Hong, K. Bartkowiak, K. Pantel
Analysis and interpretation of data (e.g., statistical analysis, biostatistics, computational analysis): M. Croset, F. Pantano, C.W.S. Kan, F. Descotes, C.-H. Lecellier, K. Pantel, P. Clézardin
Writing, review, and/or revision of the manuscript: M. Croset, F. Pantano, C.W.S. Kan, E. Bonnelye, F. Descotes, C. Alix-Panabières, K. Pantel, P. Clézardin

References

1. Hofbauer LC, Rachner TD, Coleman RE, Jakob F. Endocrine aspects of bone metastases. Lancet Diabetes Endocrinol 2014;2:500–12.
2. Coleman R, Gnant M, Morgan G, Clézardin P. Effects of bone-targeted agents on cancer progression and mortality. J Natl Cancer Inst 2012;104: 1059–67.
3. Croucher PI, McDonald MM, Martin TJ. Bone metastasis: the importance of the neighbourhood. Nat Rev Cancer 2016;16:373–86.
4. Oskarsson T, Batlle E, Massagué J. Metastatic stem cells: sources, niches, and vital pathways. Cell Stem Cell 2014;14:306–21.
5. Wang H, Yu C, Gao X, Welte T, Muscarella AM, Tian L, et al. The osteogenic niche promotes early-stage bone colonization of disseminated breast cancer cells. Cancer Cell 2015;27:193–210.
6. Ma L. MicroRNA and metastasis. Adv Cancer Res 2016;132:165–207.
7. Adams BD, Parsons C, Walker L, Zhang WC, Slack FJ. Targeting noncoding RNAs in disease. J Clin Invest 2017;127:761–71.
8. Croset M, Goehrig D, Frackowiak A, Bonnelye E, Ansieau S, Puisieux A, et al. TWIST1 expression in breast cancer cells facilitates bone metastasis formation. J Bone Miner Res 2014;29:1886–99.
9. Sahay D, Leblanc R, Grunewald TG, Ambatipudi S, Ribeiro J, Clézardin P, et al. The LPA1/ZEB1/miR-21-activation pathway regulates metastasis in basal breast cancer. Oncotarget 2015;6:20604–20.
10. Browne G, Taipaleenmäki H, Stein GS, Stein JL, Lian JB. MicroRNAs in the control of metastatic bone disease. Trends Endocrinol Metab 2014;25: 320–7.
11. Croset M, Kan C, Clézardin P. Tumour-derived miRNAs and bone metastasis. Bonekey Rep 2015;4:688.
12. Ell B, Mercatali L, Ibrahim T, Campbell N, Schwarzenbach H, Pantel K, et al. Tumor-induced osteoclast miRNA changes as regulators and biomarkers of osteolytic bone metastasis. Cancer Cell 2013;24:542–56.
13. Schild T, Low V, Blenis J, Gomes AP. Unique metabolic adaptations dictate distal organ-specific metastatic colonization. Cancer Cell 2018; 33:347–354.
14. Bellahcène A, Bachelier R, Detry C, Lidereau R, Clézardin P, Castronovo V. Transcriptome analysis reveals an osteoblast-like phenotype for human osteotropic breast cancer cells. Breast Cancer Res Treat 2007;101:135–48.
15. Le Gall C, Bellahcène A, Bonnelye E, Gasser JA, Castronovo V, Green J, et al. A cathepsin K inhibitor reduces breast cancer induced osteolysis and skeletal tumor burden. Cancer Res 2007;67:9894–902.
16. Wu T, Zhou H, Hong Y, Li J, Jiang X, Huang H. miR-30 family members negatively regulate osteoblast differentiation. J Biol Chem 2012;287: 7503–11.

17. Zhang Y, Xie R, Croce CM, Stein JL, Lian JB, van Wijnen AJ, et al. A program of microRNAs controls osteogenic lineage progression by targeting transcription factor Runx2. Proc Natl Acad Sci 2011;108: 9863–8.
18. Yang SJ, Yang SY, Wang DD, Chen X, Shen HY, Zhang XH, et al. The miR-30 family: versatile players in breast cancer. Tumor Biol 2017;39:1–13.
19. Boufraqech M, Nilubol N, Zhang L, Gara SK, Sadowski SM, Mehta A, et al. miR30a inhibits LOX expression and anaplastic thyroid cancer progression. Cancer Res 2015;75:367–77.
20. Liu M, Huang F, Zhang D, Ju J, Wu XB, Wang Y, et al. Heterochromatin protein HP1γ promotes colorectal cancer progression and is regulated by miR-30a. Cancer Res 2015;75:4593–604.
21. Zhang R, Yan S, Wang J, Deng F, Guo Y, Li Y, et al. MiR-30a regulates the proliferation, migration, and invasion of human osteosarcoma by targeting Runx2. Tumour Biol 2016;37:3479–88.
22. Zhang N, Wang X, Huo Q, Sun M, Cai C, Liu Z, et al. MicroRNA-30a suppresses breast tumor growth and metastasis by targeting metadherin. Oncogene 2014;33:3119–28.
23. Wei W, Yang Y, Cai J, Cui K, Li RX, Wang H, et al. MiR-30a-5p suppresses tumor metastasis of human colorectal cancer by targeting ITGB3. Cell Physiol Biochem 2016;39:1165–76.
24. Sun X, Zhao S, Li H, Chang H, Huang Z, Ding Z, et al. MicroRNA-30b suppresses epithelial-mesenchymal transition and metastasis of hepatoma cells. J Cell Physiol 2017;232:625–34.
25. Zhang Q, Yu L, Qin D, Huang R, Jiang X, Zou C, et al. Role of microRNA-30c targeting ADAM19 in colorectal cancer. PLoS One 2015;10:e0120698.
26. Bockhorn J, Dalton R, Nwachukwu C, Huang S, Prat A, Yee K, et al. MicroRNA-30c inhibits human breast tumour chemotherapy resistance by regulating TWF1 and IL-11. Nat Commun 2013;4:1393.
27. Zhao J-J, Lin J, Zhu D, Wang X, Brooks D, Chen M, et al. miR-30–5p functions as a tumor suppressor and novel therapeutic tool by targeting the oncogenic Wnt/β-catenin/BCL9 pathway. Cancer Res 2014;74: 1801–13.
28. Rodríguez-González FG, Sieuwerts AM, Smid M, Look MP, Meijer-van Gelder ME, de Weerd V, et al. MicroRNA-30c expression level is an independent predictor of clinical benefit of endocrine therapy in advanced estrogen receptor positive breast cancer. Breast Cancer Res Treat 2011;127: 43–51.
29. Dobson JR, Taipaleenmäki H, Hu YJ, Hong D, van Wijnen AJ, Stein JL, et al. hsa-mir-30c promotes the invasive phenotype of metastatic breast cancer cells by targeting NOV/CCN3. Cancer Cell Int 2014;14:73.

30. Gaziel-Sovran A, Segura MF, Di Micco R, Collins MK, Hanniford D, Vega-Saenz de Miera E, et al. miR-30b/30d regulation of GalNAc transferases enhances invasion and immunosuppression during metastasis. Cancer Cell 2011;20:104–18.

31. Feng G, Shi H, Li J, Yang Z, Fang R, Ye L, et al. MiR-30e suppresses proliferation of hepatoma cells via targeting prolyl 4-hydroxylase subunit alpha-1 (P4HA1) mRNA. Biochem Biophys Res Commun 2016;472:516–22.

32. Pécheur I, Peyruchaud O, Serre C-M, Guglielmi J, Voland C, Bourre F, et al. Integrin alpha(v)beta3 expression confers on tumor cells a greater propensity to metastasize to bone. FASEB J 2002;16:1266–8.

33. Pantel K, Dickmanns A, Zippelius A, Klein C, Shi J, Hoechtlen-Vollmar W, et al. Establishment of micrometastatic carcinoma cell lines: a novel source of tumor cell vaccines. J Natl Cancer Inst 1995;87:1162–8.

34. Bartkowiak K, Kwiatkowski M, Buck F, Gorges TM, Nilse L, Assmann V, et al. Disseminated tumor cells persist in the bone marrow of breast cancer patients through sustained activation of the unfolded protein response. Cancer Res 2015;75:5367–77.

35. Berthier A, Seguin S, Sasco AJ, Bobin JY, De Laroche G, Datchary J, et al. High expression of gabarapl1 is associated with a better outcome for patients with lymph node-positive breast cancer. Br J Cancer 2010;102:1024–31.

36. Fradet A, Sorel H, Bouazza L, Goehrig D, Dépalle B, Bellahcène A, et al. Dual function of ERRα in breast cancer and bone metastasis formation: implication of VEGF and osteoprotegerin. Cancer Res 2011;71:5728–38.

37. Bonnelye E, Merdad L, Kung V, Aubin JE. The orphan nuclear estrogen receptor-related receptor alpha (ERRalpha) is expressed throughout osteoblast differentiation and regulates bone formation in vitro. J Cell Biol 2001;153:971–84.

38. Gamez-Pozo A, Berges-Soria J, Arevalillo JM, Nanni P, López-Vacas R, Navarro H, et al. Combined label-free quantitative proteomics and microRNA expression analysis of breast cancer unravel molecular differences with clinical implications. Cancer Res 2015;75:2243–53.

39. Yu F, Yao H, Zhu P, Zhang X, Pan Q, Gong C, et al. let-7 regulates self renewal and tumorigenicity of breast cancer cells. Cell 2007;131:1109–23.

40. Huang CF, Lira C, Chu K, Bilen MA, Lee YC, Ye X, et al. Cadherin-11 increases migration and invasion of prostate cancer cells and enhances their interaction with osteoblasts. Cancer Res 2010;70:4580–9.

41. Chen PS, Wang MY, Wu BSN, Su JL, Hong CC, Chuang SE, et al. CTGF enhances the motility of breast cancer cells via an integrin-avb3–ERK1/2-dependent S100A4-upregulated pathway. J Cell Science 2007;120:2053–65.

42. Esquela-Kerscher A, Slack FJ. Oncomiirs - microRNAs with a role in cancer. Nat Rev Cancer 2006;6:259–69.

43. Kuchenbauer F, Mah SM, Heuser M, McPherson A, Rüschmann J, Rouhi A, et al. Comprehensive analysis of mammalian miRNA* species and their role in myeloid cells. Blood 2011;118:3350–8.

44. Hassan MQ, Maeda Y, Taipaleenmaki H, Zhang W, Jafferji M, Gordon JA, et al. miR-218 directs a Wnt signaling circuit to promote differentiation of osteoblasts and osteomimicry of metastatic cancer cells. J Biol Chem 2012;287:42084–92.

45. Tamura D, Hiraga T, Myoui A, Yoshikawa H, Yoneda T. Cadherin-11-mediated interactions with bone marrow stromal/osteoblastic cells support selective colonization of breast cancer cells in bone. Int J Oncol 2008;33:17–24.

46. Chu K, Cheng CJ, Ye X, Lee YC, Zurita AJ, Chen DT, et al. Cadherin-11 promotes the metastasis of prostate cancer cells to bone. Mol Cancer Res 2008;6:1259–67.

47. Brümmer A, Hausser J. MicroRNA binding sites in the coding region of mRNAs: extending the repertoire of post-transcriptional gene regulation. Bioessays 2014;36:617–26.

48. Taipaleenmäki H, Browne G, Akech J, Zustin J, van Wijnen AJ, Stein JL, et al. Targeting of Runx2 by miR-135 and miR-203 impairs progression of breast cancer and metastatic bone disease. Cancer Res 2015;75:1433–44.

49. Ju JA, Godet I, Ye IC, Byun J, Jayatilaka H, Lee SJ, et al. Hypoxia selectively enhances integrin $\alpha5/\beta1$ receptor expression in breast cancer to promote metastasis. Mol Cancer Res 2017;15:723–34.

50. Qin L, Chen X, Wu Y, Feng Z, He T, Wang L, et al. Steroid receptor coactivator-1 upregulates integrin α_5 expression to promote breast cancer cell adhesion and migration. Cancer Res 2011;71:1742–51.

51. Li XQ, Lu JT, Tan CC, Wang QS, Feng YM. RUNX2 promotes breast cancer bone metastasis by increasing integrin $\alpha5$-mediated colonization. Cancer Lett 2016;380:78–86.

52. Kang Y, Siegel PM, Shu W, Drobnjak M, Kakonen SM, Cordón-Cardo C, et al. A multigenic program mediating breast cancer metastasis to bone. Cancer Cell 2003;3:537–49.

53. Zhao Y, Bachelier R, Treilleux I, Pujuguet P, Peyruchaud O, Baron R, et al. Tumor alphavbeta3 integrin is a therapeutic target for breast cancer bone metastases. Cancer Res 2007;67:5821–30.

54. Duisters RF, Tijsen AJ, Schroen B, Leenders JJ, Lentink V, van der Made I, et al. miR-133 and miR-30 regulate connective tissue growth factor: implications for a role of microRNAs in myocardial matrix remodeling. Circ Res 2009;104:170–8.